

4E-BP2–dependent translation in parvalbumin neurons controls epileptic seizure threshold

Vijendra Sharma^{a,b,1}, Rapita Sood^{a,b}, Danning Lou^{a,b}, Tzu-Yu Hung^{a,b}, Maxime Lévesque^c, Yelin Han^{a,b}, Jeremy Y. Levett^{a,b}, Peng Wang^{a,b}, Shrvan Murthy^{a,b}, Shannon Tansley^d, Siyan Wang^c, Nadeem Siddiqui^{a,b}, Soroush Tahmasebi^e, Kobi Rosenblum^f, Massimo Avoli^g, Jean-Claude Lacaille^h, Nahum Sonenberg^{a,b,1}, and Arkady Khoutorsky^{d,1}

^aDepartment of Biochemistry, McGill University, Montreal, QC H3A 2B4, Canada; ^bRosalind and Morris Goodman Cancer Research Centre, McGill University, Montreal, QC H3A 2B4, Canada; ^cMontreal Neurological Institute and Hospital, Department of Neurology & Neurosurgery, McGill University, Montreal, QC H3A 2B4, Canada; ^dDepartment of Anesthesia and Faculty of Dentistry, McGill University, Montreal, QC H3A 2B4, Canada; ^eDepartment of Pharmacology and Regenerative Medicine, University of Illinois at Chicago, Chicago, IL 60612; ^fSagol Department of Neurobiology, University of Haifa, Mount Carmel, Haifa, 3498838, Israel; ^gMontreal Neurological Institute and Hospital, Department of Physiology, McGill University, Montreal, QC H3A 2B4, Canada; and ^hDepartment of Neurosciences, Centre for Interdisciplinary Research on Brain and Learning, Research Group on the Central Nervous System, Université de Montréal, Montréal, QC H3C 3J7, Canada

Contributed by Nahum Sonenberg, February 15, 2021 (sent for review December 11, 2020; reviewed by Eric Klann and Mustafa Sahin)

The mechanistic/mammalian target of rapamycin complex 1 (mTORC1) integrates multiple signals to regulate critical cellular processes such as mRNA translation, lipid biogenesis, and autophagy. Germline and somatic mutations in mTOR and genes upstream of mTORC1, such as *PTEN*, *TSC1/2*, *AKT3*, *PIK3CA*, and components of GATOR1 and KICSTOR complexes, are associated with various epileptic disorders. Increased mTORC1 activity is linked to the pathophysiology of epilepsy in both humans and animal models, and mTORC1 inhibition suppresses epileptogenesis in humans with tuberous sclerosis and animal models with elevated mTORC1 activity. However, the role of mTORC1-dependent translation and the neuronal cell types mediating the effect of enhanced mTORC1 activity in seizures remain unknown. The eukaryotic translation initiation factor 4E-binding protein 1 (4E-BP1) and 2 (4E-BP2) are translational repressors downstream of mTORC1. Here we show that the ablation of 4E-BP2, but not 4E-BP1, in mice increases the sensitivity to pentylenetetrazole (PTZ)- and kainic acid (KA)-induced seizures. We demonstrate that the deletion of 4E-BP2 in inhibitory, but not excitatory neurons, causes an increase in the susceptibility to PTZ-induced seizures. Moreover, mice lacking 4E-BP2 in parvalbumin, but not somatostatin or VIP inhibitory neurons exhibit a lowered threshold for seizure induction and reduced number of parvalbumin neurons. A mouse model harboring a human *PIK3CA* mutation that enhances the activity of the PI3K-AKT pathway (*Pik3ca*^{H1047R-Pvalb}) selectively in parvalbumin neurons shows susceptibility to PTZ-induced seizures. Our data identify 4E-BP2 as a regulator of epileptogenesis and highlight the central role of increased mTORC1-dependent translation in parvalbumin neurons in the pathophysiology of epilepsy.

mRNA translation | epilepsy | mTORC1

Epilepsy is a prevalent (0.5 to 1% of the general population) (1) heterogeneous neurological disorder affecting all age groups and is characterized by seizures and associated psychological and social stigmas (2–4). Hyperactivation of the mechanistic/mammalian target of rapamycin (mTOR) pathway has been reported in brain lesions of epileptic patients with neurodevelopmental disorders (5, 6), and human genetic studies have shown that mutations in mTOR (7, 8) and other components of its pathway are linked to epileptogenesis (6, 9–13). mTOR is a highly conserved serine/threonine protein kinase that forms two distinct complexes: mTORC1 and mTORC2. mTORC1 integrates multiple environmental and intracellular signals to modulate brain functions by controlling key cellular processes such as mRNA translation, nucleotide, lipid and mitochondrial biogenesis, and autophagy (14, 15). Germline or somatic mutations, which result in enhanced mTORC1 activity, including in *PIK3CA*, *PTEN*, *AKT3*, *TSC1/2*, *RHEB*, and *MTOR*, are associated with

neurodevelopmental disorders with epilepsy (16–23). Recent studies have also identified mutations in mTORC1 upstream amino acid-sensing GATOR1-KICSTOR-Rag GTPase pathways as a common cause of epilepsy (24), revealing that mutations in GATOR1 (*DEPDC5*, *NPRL2*, and *NPRL3*) (25, 26) and KICSTOR (*ITFG2*, *KPTN*, *SZT2*, and *C12ORF66*) (6, 7, 27) genes are often found in epileptic pathologies. The link between the mTORC1 and epilepsy has been recapitulated in animal models with enhanced mTORC1 activity (e.g., *Pten*^{+/-}, *TSC1/2*^{+/-}, and activating mutations in *Pik3ca* Nestin-Cre knockin (KI), *Akt3* KI, *MTOR*, and *Rheb* KI) (18, 20, 23, 28–31) while inhibition of mTORC1 reversed epileptogenesis in *TSC1*^{GFAP-Cre} and *Pten*^{+/-} mice (20, 31). Notably, the mTORC1 rapalog, everolimus, has been approved by the US Food and Drug Administration (FDA) for the treatment of epilepsy in tuberous sclerosis complex (TSC) patients (32, 33).

mTORC1 is a master regulator of mRNA translation. Upon activation, mTORC1 phosphorylates S6 protein kinases 1 and 2 (S6K1/2) and 4E-binding proteins (4E-BPs) (34, 35). In the

Significance

In numerous models of neurodevelopmental disorders and epilepsy, genetic mutations associated with enhanced mTORC1 activity engender an increase in the susceptibility to epileptic seizures. This study shows that the deletion of the mTORC1-downstream translational repressor, 4E-BP2, but not 4E-BP1, promotes epileptogenesis. By deleting 4E-BP2 in different cell types, we reveal that the up-regulation of mTORC1/eIF4E signaling in parvalbumin inhibitory neurons is sufficient to reduce the threshold for the induction of seizures. We conclude that downstream of mTORC1, 4E-BP2 is the main 4E-BP paralog controlling epileptogenesis and propose that parvalbumin inhibitory neurons are a vulnerable cell type in which the aberrant activation of mTORC1-dependent translation contributes to epileptic pathology.

Author contributions: V.S., R.S., M.L., N. Siddiqui, S. Tahmasebi, K.R., M.A., J.-C.L., N. Sonenberg, and A.K. designed research; V.S., R.S., D.L., T.-Y.H., M.L., Y.H., J.Y.L., P.W., S.M., S. Tansley, S.W., N. Siddiqui, M.A., and N. Sonenberg performed research; S. Tahmasebi and N. Sonenberg contributed new reagents/analytic tools; V.S., R.S., M.L., M.A., and N. Sonenberg analyzed data; and V.S., R.S., N. Sonenberg, and A.K. wrote the paper.

Reviewers: E.K., New York University; and M.S., Boston Children's Hospital/Harvard Medical School.

The authors declare no competing interest.

Published under the PNAS license.

¹To whom correspondence may be addressed. Email: vijendra.sharma@mcgill.ca, nahum.sonenberg@mcgill.ca, or arkady.khoutorsky@mcgill.ca.

Published April 5, 2021.

hypophosphorylated form, 4E-BPs bind and prevent the association of the cap-binding protein eIF4E with the large scaffolding protein eIF4G, thereby inhibiting the formation of the eIF4F complex (composed of eIF4E, eIF4G, and an mRNA helicase eIF4A), which is essential for the initiation of cap-dependent translation. Phosphorylation of 4E-BPs by mTORC1 results in the release of eIF4E from 4E-BPs, allowing eIF4F complex formation and initiation of translation (36, 37). Among the three 4E-BP family members (4E-BP1, 4E-BP2, and 4E-BP3), 4E-BP2 is the most abundant paralog in the mammalian brain (38, 39). A recent study (5) has identified aberrant activation of eIF4E as a major mechanism for translational changes in focal malformations of cortical development (FMCD), a condition that is often caused by brain somatic activating mutations in *MTOR* and presents with intractable epilepsy in children, accompanied by developmental abnormalities and autism spectrum disorder (ASD) (5, 40–42). Increased eIF4E activity has a pathogenic role in inducing epileptic seizures in FMCD as eIF4E knockdown prevented spontaneous seizures in mTOR Cys1483Tyr and Leu2427Pro mutant mice (5), which show mTORC1 hyperactivation.

Despite the progress in understanding the causal link between enhanced mTORC1 activity and epilepsy, the mTORC1-downstream molecular mechanisms promoting epileptogenesis and the cell types mediating the effect on seizure threshold and severity remain poorly understood. In this work, we investigated the role of two main mTORC1-downstream effectors, 4E-BP1 and 4E-BP2, in regulating seizure susceptibility and studied the neuronal cell types mediating epileptogenic effects. We report that mice with whole-body or parvalbumin neuron-specific deletion of 4E-BP2 exhibit reduced threshold and increased severity of epileptic seizures. Moreover, we show that *Pik3ca^{H1047R-Pvalb}* mutant mice harboring a conditional parvalbumin neuron-specific KI gain-of-function mutation (*H1047R*) in the *PIK3CA* kinase domain are prone to seizures. Collectively, these findings demonstrate a central role of 4E-BP2 and parvalbumin neurons in mediating mTORC1-dependent epileptogenesis, thus expanding our understanding of cell type-specific molecular mechanisms of translation dysregulation in epilepsy and other neurodevelopmental disorders.

Results

Susceptibility to PTZ-Induced Seizures Is Increased in *Eif4ebp1/2/3* Knockout Mice. To study the role of 4E-BPs in epileptogenesis, we first determined behavioral seizure responses in mice lacking all three 4E-BP paralogs, 4E-BP1, 4E-BP2, and 4E-BP3 (*Eif4ebp^{-/-/-}*) (43). We used a well-established model of epilepsy, in which seizures are induced by the convulsant drug pentylenetetrazole (PTZ), a gamma-aminobutyric acid type A receptors (GABA_ARs) antagonist (44). *Eif4ebp^{-/-/-}* mice, lacking 4E-BPs (Fig. 1A), were administered with increasing doses of PTZ (50, 60, and 70 mg/kg, subcutaneously [s.c.]) and monitored for 30 min postinjection to measure mortality, latency to the first seizure, and duration of epileptic tonic-clonic seizures (Fig. 1B). *Eif4ebp^{-/-/-}* mice injected with 70 mg/kg of PTZ exhibit a dramatically shorter onset to develop generalized seizures (*Eif4ebp^{-/-/-}* mice, 2.91 ± 0.45 ; *Eif4ebp^{+/+}*, 7.01 ± 0.75 ; mean [time in minutes] \pm SEM), increased cumulative seizure duration (an increase of $111.73 \pm 20.05\%$), and increased mortality (75% of *Eif4ebp^{-/-/-}* mice as compared with 25% in wild type [WT]) (Fig. 1C–G). We conclude that the deletion of 4E-BPs reduces PTZ-induced seizure threshold and increases seizure-associated mortality.

Increased Sensitivity to PTZ-Induced Seizures in *Eif4ebp2* Knockout Mice. Since the deletion of all three 4E-BPs resulted in a lowered threshold for PTZ-induced seizures in *Eif4ebp^{-/-/-}* mice, we investigated which 4E-BP paralog mediates the enhanced sensitivity to PTZ-induced seizures in mice (4E-BP3 is not detected in the brain) (45). First, we determined the threshold for PTZ-

induced seizures in 4E-BP1 knockout mice (*Eif4ebp1^{-/-}*) by measuring the response to the administration of 70 mg/kg of PTZ. The deletion of 4E-BP1 was insufficient to reduce the threshold for seizure onset or to increase the seizure duration (Fig. 1H–K) as behavioral responses to PTZ were similar in *Eif4ebp1^{-/-}* and control (*Eif4ebp1^{+/+}*) mice. We then examined the contribution of 4E-BP2 to ictogenesis by pharmacologically inducing acute seizures with PTZ (70 mg/kg) in *Eif4ebp2^{-/-}* mice (Fig. 1L–O). 4E-BP2 deletion resulted in a substantial decrease in seizure latency (reduced by $52.12 \pm 4.83\%$), prolonged seizure duration (an increase of $91.8 \pm 23.42\%$; Fig. 1L–O), and increased mortality (88.24% of *Eif4ebp^{-/-}* mice as compared with 15% in WT; Fig. 1L–O). Taken together, our results show that 4E-BP2, the predominant isoform in the mammalian brain (12, 38), but not 4E-BP1, plays a central role in determining susceptibility to epileptic seizures.

Altered Kainic Acid–Induced Seizures Sensitivity in *Eif4ebp2* Knockout Mice. To corroborate the role of 4E-BP2 in epileptogenesis, we used escalating doses of kainic acid (KA; 10, 20, and 30 mg/kg injected subcutaneously) to induce seizures in *Eif4ebp2^{-/-}* mice (Fig. 2A–D). KA is a potent agonist of the kainate class of ionotropic glutamate receptors (46). Administration of 30 mg/kg KA in *Eif4ebp2^{-/-}* mice led to a shorter latency to the first seizure ($59.52 \pm 8.3\%$ reduced onset; Fig. 2C) and extended seizure duration ($99.15 \pm 29.43\%$ increase; Fig. 2D) as compared with control *Eif4ebp2^{+/+}* mice. These results provide compelling evidence that the deletion of 4E-BP2 augments seizure susceptibility.

Selective Ablation of *Eif4ebp2* in Inhibitory Neurons Alters PTZ-Evoked Seizure Threshold. To investigate which neuronal cell types mediate the effect of 4E-BP2 ablation on seizure susceptibility, we generated excitatory neuron-specific conditional knockout mice *Eif4ebp2^{flx/flx};Emx1-Cre⁺* (cKO^{Emx1}; Fig. 2E), in which Cre recombinase is expressed under the control of the *Emx1* promoter. In cKO^{Emx1} mice, 4E-BP2 is ablated during early development (embryonic day [E] 12.5) in EMX1-expressing excitatory neurons (EMX1⁺). Immunofluorescence (IF) colabeling of 4E-BP2 and excitatory neuron-specific marker (CAMK2 α) confirmed the deletion of 4E-BP2 in excitatory neurons of cKO^{Emx1} animals (Fig. 2F). To study the effect of *Eif4ebp2* deletion in EMX1⁺ neurons on epileptogenesis, we evoked seizures by injecting 70 mg/kg of PTZ in WT^{Emx1} and cKO^{Emx1} mice. We observed similar latencies to develop epileptic seizures and equal seizure durations in WT^{Emx1} and cKO^{Emx1} animals (Fig. 2G–I). Next, we used the *Camk2a* promoter to express Cre, which results in the deletion of 4E-BP2 in CAMK2 α -expressing excitatory neurons (CAMK2 α ⁺; Fig. 2J) during the postnatal developmental stage. We observed no change in PTZ-evoked seizure parameters (mortality, onset and duration of seizure; Fig. 2K–M) between *Eif4ebp2^{flx/flx};Camk2a-Cre⁺* mice (cKO^{Camk2 α}) and wild-type control *Eif4ebp2^{+/+};Camk2a-Cre⁺* mice (WT^{Camk2 α}). Thus, these results show that the deletion of 4E-BP2 in excitatory neurons does not promote epileptogenesis.

To study the impact of the deletion of *Eif4ebp2* in GABAergic inhibitory neurons at different developmental stages, we crossed floxed *Eif4ebp2^{flx/flx}* mice with mice expressing the Cre recombinase under the control of the *Nkx2.1* promoter, which switches on at E10.5 in inhibitory neurons (47) or mice expressing Cre under the control of the *Gad2* promoter, which switches on at postnatal day 6 (P6) (48). We confirmed by IF the inhibitory neuron-specific ablation of 4E-BP2 in both conditional knockout mouse models: *Eif4ebp2^{flx/flx};Nkx2.1-Cre⁺* (cKO^{Nkx2.1}; Fig. 2N) and *Eif4ebp2^{flx/flx};Gad2-Cre⁺* (cKO^{Gad2}; Fig. 2R). We injected PTZ (70 mg/kg) to evoke seizures in cKO^{Nkx2.1} and cKO^{Gad2} mice and their respective wild-type controls (*Eif4ebp2^{+/+};Nkx2.1-Cre⁺* [WT^{Nkx2.1}] and *Eif4ebp2^{+/+};Gad2-Cre⁺* [WT^{Gad2}] mice). Importantly, conditional deletion of *Eif4ebp2* in either NKX2.1⁺ or

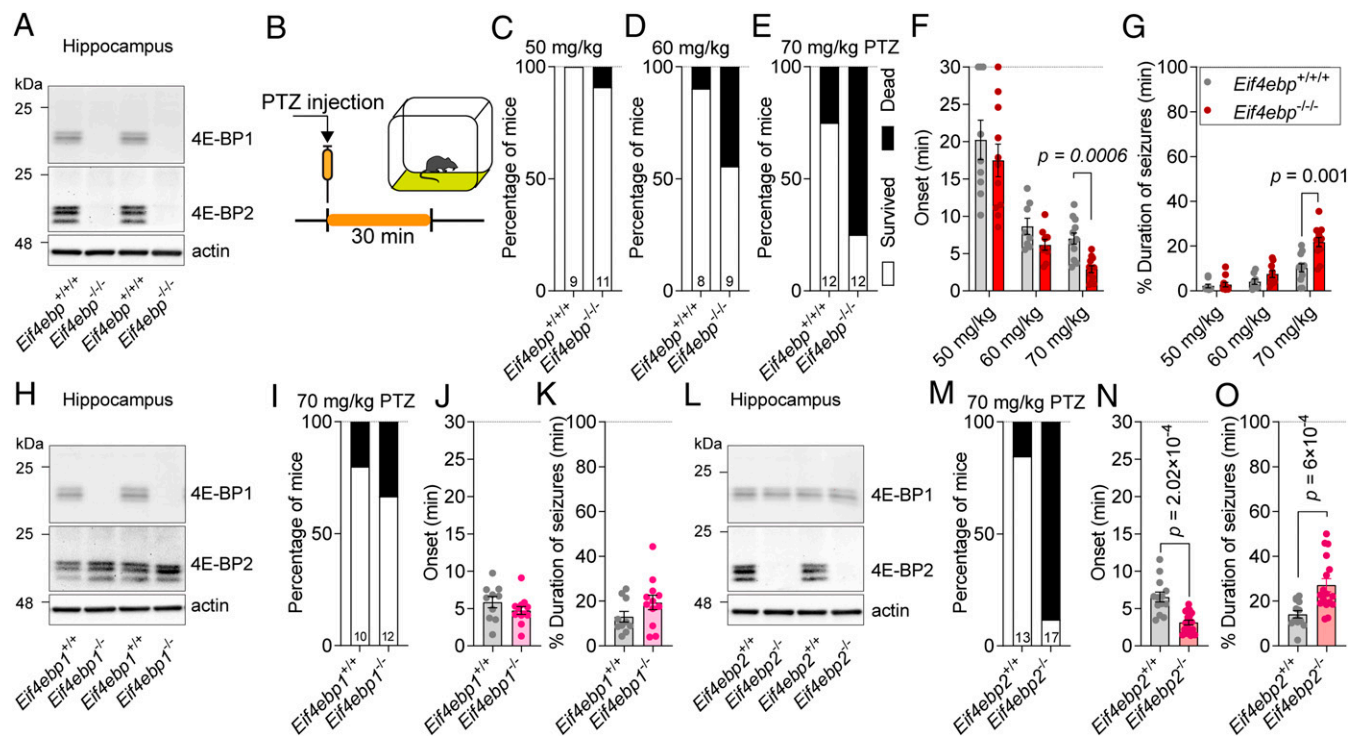


Fig. 1. Deletion of *Eif4ebp1/2/3* and *Eif4ebp2* alters susceptibility to PTZ-induced seizures. (A) Representative Western blot of hippocampal tissue from *Eif4ebp1/2/3* triple knockout (*Eif4ebp^{-/-}*) mice showing ablation of 4E-BP1 and 4E-BP2 (4E-BP3 was not detected in the brain). (B) Timeline of PTZ injection and videorecorded observations. Seizure incidence was measured by scoring seizure behaviors in mice. (C–E) *Eif4ebp^{-/-}* mice were injected with different concentrations of PTZ (50, 60, and 70 mg/kg s.c.), and the percentage of mice that survived or died 30 min post-PTZ injection was quantified. (F) Latency to the first PTZ-induced tonic-clonic seizure at different PTZ concentrations (mixed-effects model [REML]; $F_{1,55} = 6.426$, $P = 0.0141$). The latency to the first seizure (onset) in response to 70 mg/kg of PTZ was significantly shorter in *Eif4ebp^{-/-}* mice than the wild-type control (Sidak's multiple comparisons test, $P = 0.0006$, $n = 12$, 12). (G) Cumulative percentage duration of seizures in *Eif4ebp^{-/-}* and wild-type mice after s.c. injection of different concentrations of PTZ (mixed-effects model [REML]; $F_{1,55} = 15.89$, $P = 0.0002$). Seizures were recorded for 30 min after PTZ injection. Cumulative seizure percentage duration in response to 70 mg/kg PTZ injection is longer in *Eif4ebp^{-/-}* mice than in wild-type mice (Sidak's multiple comparisons test, $P = 0.001$, $n = 12$, 12). (H) Immunoblots of hippocampal protein lysate from *Eif4ebp1* knockout mice showing 4E-BP1 ablation. (I–K) *Eif4ebp1* knockout (*Eif4ebp1^{-/-}*) mice have similar mortality, seizure onset ($t_{16,69} = 1.186$, $P = 0.252$, $n = 10$, 12) and percentage of seizures ($t_{19,35} = 1.594$, $P = 0.127$, $n = 10$, 12) for PTZ-induced seizure as control. (L) Immunoblot of hippocampal lysates from *Eif4ebp2* knockout (*Eif4ebp2^{-/-}*) mice shows the deletion of 4E-BP2. (M–O) The dose of 70 mg/kg of PTZ caused more mortality, reduced seizure onset ($t_{17,54} = 4.674$, $P = 2.02 \times 10^{-4}$, $n = 13$, 18), and increased the percentage duration of seizures ($t_{24,37} = 3.915$, $P = 6 \times 10^{-4}$, $n = 13$, 17) in *Eif4ebp2^{-/-}* mice. A two-tailed unpaired *t* test with Welch's correction was used to compare two groups. Data are mean \pm SEM.

GAD2⁺ inhibitory neurons lowers the threshold for PTZ-evoked seizures (onset of seizure reduced by $65.57 \pm 6.4\%$ in $cKO^{Nkx2.1}$ and $57.31 \pm 4.62\%$ in cKO^{Gad2}), increases the duration of seizures (an increase of $118.96 \pm 29.33\%$ in $cKO^{Nkx2.1}$ and $80.49 \pm 19.13\%$ in cKO^{Gad2}), and elevates mortality in $cKO^{Nkx2.1}$ (Fig. 2 O–Q) and cKO^{Gad2} animals (Fig. 2 S–U) as compared with control groups. These results demonstrate that the ablation of 4E-BP2 in inhibitory (prenatal and postnatal), but not excitatory neurons is sufficient to promote ictogenesis.

Loss of 4E-BP2 in Parvalbumin Neurons Increases PTZ-Induced Seizure Severity. We further investigated the subtypes of inhibitory neurons via which 4E-BP2 ablation contributes to epileptic seizures. To this end, we crossed *Eif4ebp2^{flx/flx}* mice with three major inhibitory neuron-specific Cre lines to delete 4E-BP2 in the somatostatin (SST⁺), vasoactive intestinal peptide (VIP⁺), and parvalbumin (PVALB⁺)-expressing subtypes of GABAergic inhibitory neurons. Similar PTZ-induced latency to develop epileptic seizure, mortality, and duration of convulsive episodes, were observed in *Eif4ebp2^{flx/flx};Sst-Cre⁺* (cKO^{Sst} ; Fig. 3 A–D) and *Eif4ebp2^{flx/flx};VIP-Cre⁺* mice (cKO^{VIP} ; Fig. 3 E–H) as compared with their respective wild-type controls. However, genetic elimination of *Eif4ebp2* in PVALB⁺ neurons lowered the threshold for PTZ-evoked seizures, as evidenced by shortening of latency (reduced by $50.05 \pm 6.26\%$), increase in mortality rate, and prolongation of

epileptic activities in *Eif4ebp2^{flx/flx};Pvalb-Cre⁺* mice (cKO^{Pvalb} ; $101.3 \pm 23.58\%$ increase in seizure duration; Fig. 3 I–L) as compared with the wild-type control *Eif4ebp2^{+/+};Pvalb-Cre⁺* (WT^{*Pvalb*}) mice. Thus, ablation of 4E-BP2 in PVALB⁺ neurons is sufficient to promote epileptogenesis. To corroborate these results using a different approach, we implanted a bipolar recording electrode (see *Experimental Procedures: Electrode Implantation, EEG Recordings, and Analysis*) in the CA3 region of the hippocampus and performed electroencephalogram (EEG) recordings in the freely behaving WT^{*Pvalb*} and cKO^{Pvalb} mice treated with the convulsant PTZ (50 mg/kg). EEG signal analysis demonstrated the earlier onset of electrographic seizures in cKO^{Pvalb} mice within the first 10 min of PTZ administration ($61.74 \pm 7.8\%$ earlier; Fig. 3 M, N, and P). Moreover, the total percentage of electrographic seizure duration was increased in cKO^{Pvalb} mice (WT^{*Pvalb*} $1.89 \pm 1.12\%$ and cKO^{Pvalb} $12.5 \pm 3.92\%$ seizure duration; Fig. 3O). Next, we studied the role of 4E-BP2 in PVALB⁺ neurons in epilepsy by assessing the threshold for KA-induced seizures in cKO^{Pvalb} mice. Administration of 30 mg/kg KA in cKO^{Pvalb} mice leads to a significant shortening of latency to seizures ($67.48 \pm 3.51\%$ shorter) and increased seizure duration ($122.94 \pm 24.85\%$ more seizures; Fig. 4 A–C). Taken together, these findings show that 4E-BP2 ablation in PVALB⁺

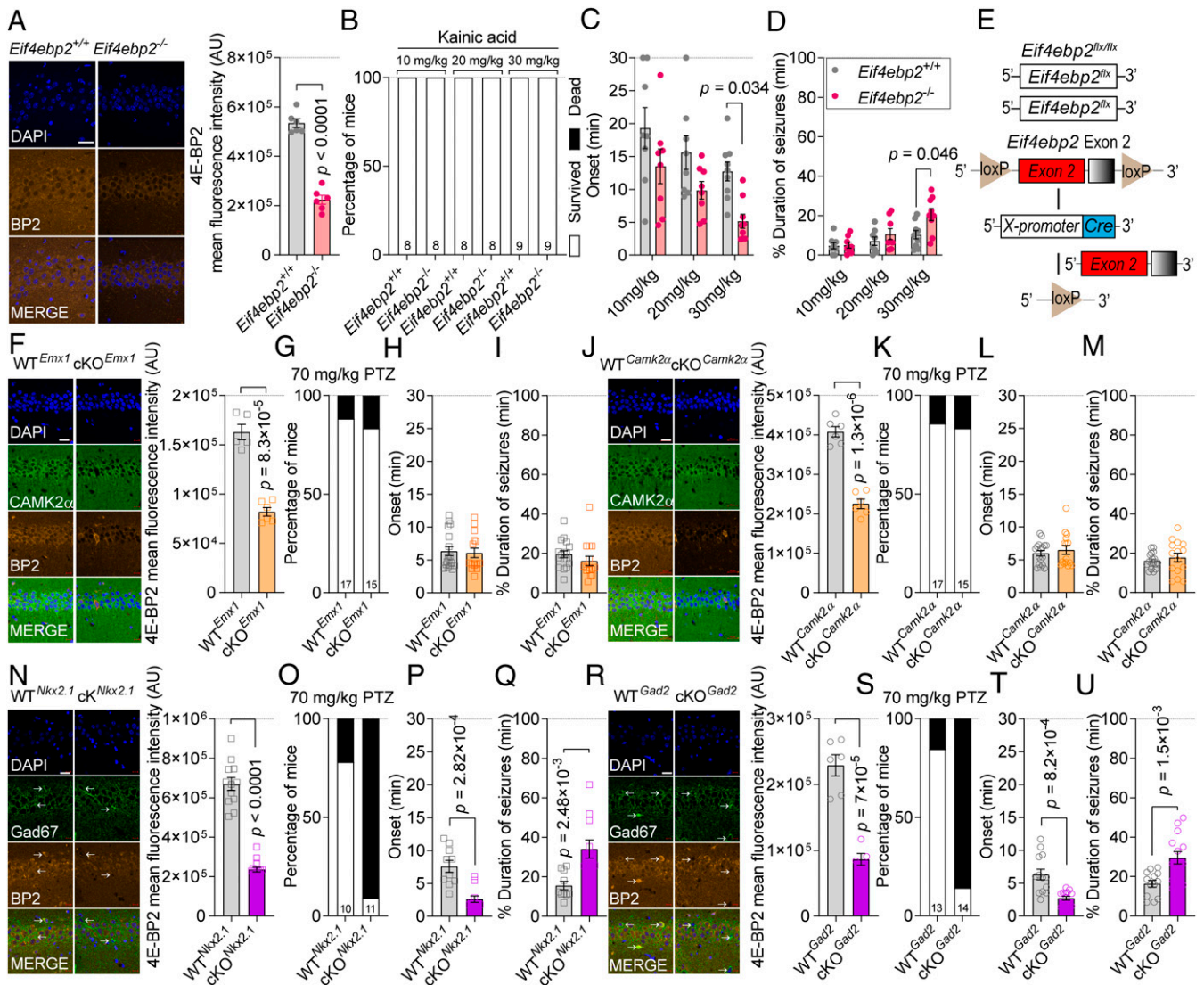


Fig. 2. Global ablation of 4E-BP2 (*Eif4ebp2* KO) and inhibitory neuron-specific ablation of 4E-BP2 (cKO^{Nkx2.1} and cKO^{Gad2}) increase seizure susceptibility. (A) Immunofluorescent labeling confirms the depletion of 4E-BP2 in *Eif4ebp2* knock-out (*Eif4ebp2*^{-/-}) mice ($t_{9.985} = 12.24$, $P < 0.0001$, $n = 6$, 6). (B–D) KA-induced dose-independent induction of epileptiform activity was not lethal but ascribe early-onset (REML; $F_{1,16} = 8.866$, $P = 8.9 \times 10^{-3}$; Sidak's multiple comparisons test, $P = 0.034$, $n = 9$, 9) and increased percentage duration of seizure events in *Eif4ebp2*^{-/-} mice (REML; $F_{1,44} = 6.098$, $P = 0.0175$; Sidak's test, $P = 0.046$, $n = 9$, 9). (E) The genetic strategy for the cell type-specific deletion of 4E-BP2. (F–I) Selective ablation of 4E-BP2 in EMX1-expressing excitatory neurons (cKO^{Emx1}; $t_{6.239} = 9.023$, $P = 8.3 \times 10^{-5}$, $n = 5$, 6) does not alter PTZ-induced mortality, the latency to the first seizure ($t_{29.65} = 0.275$, $P = 0.785$, $n = 17$, 15), and duration of convulsive behavior ($t_{26.01} = 1.154$, $P = 0.259$, $n = 17$, 15) as compared with control mice. (J–M) Deletion of 4E-BP2 in CAMK2 α -expressing excitatory neurons (cKO^{Camk2 α} ; $t_{9.924} = 10.30$, $P = 1.3 \times 10^{-6}$, $n = 6$, 6) does not change the PTZ-induced mortality, latency to the first seizure ($t_{23.77} = 0.623$, $P = 0.54$, $n = 17$, 15), and total duration of seizures ($t_{19.22} = 0.716$, $P = 0.483$, $n = 17$, 15). (N–Q) Ablation of 4E-BP2 in NKX2.1-expressing inhibitory neurons (cKO^{Nkx2.1}; $t_{4.2} = 12.27$, $P < 0.0001$, $n = 12$, 14) increases PTZ-induced mortality, reduces latency to the first seizure ($t_{13.84} = 4.82$, $P = 2.82 \times 10^{-4}$, $n = 10$, 11), and increases the duration of epileptic seizures ($t_{14.09} = 3.68$, $P = 2.48 \times 10^{-3}$, $n = 10$, 11) as compared with control mice. (R–U) Deletion of 4E-BP2 in GAD2-expressing inhibitory neurons (cKO^{Gad2}; $t_{7.597} = 7.782$, $P = 7 \times 10^{-5}$, $n = 6$, 5) enhances the susceptibility to PTZ-induced seizure onset ($t_{15.03} = 4.168$, $P = 8.2 \times 10^{-4}$, $n = 13$, 14) and prolongs the duration of generalized tonic-clonic seizures ($t_{20.28} = 3.671$, $P = 1.5 \times 10^{-3}$, $n = 13$, 14). (Scale bar, 20 μ m). The pyramidal cell layer (stratum pyramidale) of the hippocampal CA1 region was used for the immunofluorescence imaging and quantification of A, F, J, N, and R. A two-tailed unpaired *t* test with Welch's correction was used to compare two groups. Data are mean \pm SEM.

neurons results in the hyperexcitability of hippocampal CA3 circuits and reduced threshold for seizure induction.

Immunostaining of hippocampal sections with the anti-parvalbumin antibody revealed a reduction in the number of PVALB⁺ neurons (WT 60.64 ± 2.82 , 4E-BP2 cKO^{Pvalb} 50.88 ± 3.28 , $P = 0.042$, Fig. 4D) without a change in the intensity of parvalbumin staining (Fig. 4E). Parvalbumin neurons in the brain are surrounded by specialized extracellular structures, perineuronal nets (PNNs), which are composed of chondroitin sulfate proteoglycans (49) and enwrap the neuronal soma and

proximal dendrites to control neuroplasticity potential (50, 51). PNNs were visualized using wisteria floribunda agglutinin (WFA), a lectin that specifically binds *N*-acetylgalactosamine beta residues of glycoproteins within the PNNs. We observed a significant reduction in the number of PNNs in the hippocampus of adult 4E-BP2 cKO^{Pvalb} mice ($26.57 \pm 5.94\%$ reduction in PNNs density; Fig. 4F). Normalization to the total number of PVALB⁺ neurons revealed that the reduction was caused by a decrease in the number of PVALB⁺ neurons as the percentage of PVALB⁺ neurons surrounded by PNNs (WFA positive) in 4E-BP2 cKO^{Pvalb}

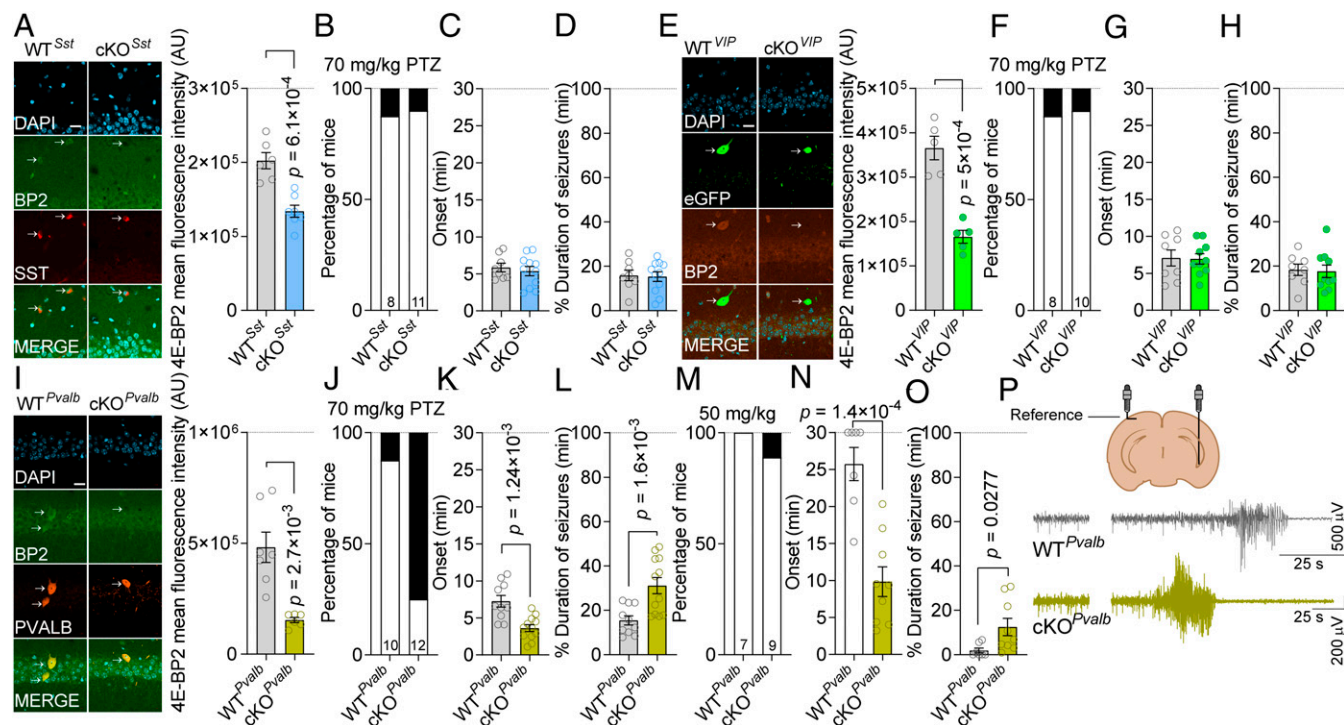


Fig. 3. *Eif4ebp2^{Pvalb}* mice exhibit increased PTZ-induced epileptic behavior and electrographic seizures. (A–D) Immunofluorescent staining shows reduced 4E-BP2 in somatostatin-expressing neurons ($t_{9.532} = 5.011$, $P = 6.12 \times 10^{-4}$, $n = 6$, 7). The threshold for PTZ (70 mg/kg)-induced behavioral seizure remains unaltered in *Eif4ebp2^{flx/flx};Sst-Cre⁺* (cKO^{Sst}) mice. Quantification of mortality, seizure onset ($t_{16.88} = 0.567$, $P = 0.578$, $n = 8$, 11) and percentage of seizures ($t_{15.78} = 0.167$, $P = 0.87$, $n = 8$, 11) shows similar results as compared with control mice (B; Dead [Black] and survived [White]). (E) The *Eif4ebp2^{flx/flx};VIP-Cre⁺* (cKO^{VIP}) mice hippocampus was injected with AAV9-EF1 α -DIO-EYFP-WPRE-hGH to label Cre-positive VIP neurons in CA1 of dorsal hippocampus. Immunofluorescent staining shows reduced 4E-BP2 in eGFP-expressing VIP neurons ($t_{6.212} = 6.599$, $P = 5.04 \times 10^{-4}$, $n = 5$, 5). (F–H) In cKO^{VIP} mice, the mortality rate, seizure onset ($t_{12.31} = 0.095$, $P = 0.926$, $n = 8$, 10), and cumulative seizure duration in response to 70 mg/kg of PTZ are similar to control ($t_{15.99} = 0.191$, $P = 0.851$, $n = 8$, 10). (I–L) In *Eif4ebp2^{flx/flx};Pvalb-Cre⁺* (cKO^{Pvalb}) mice, injection of 70 mg/kg of PTZ resulted in higher mortality and significantly reduced seizure threshold as seen in onset ($t_{14.64} = 3.99$, $P = 1.24 \times 10^{-3}$, $n = 10$, 12) and percentage duration of seizures ($t_{17.02} = 3.74$, $P = 1.6 \times 10^{-3}$, $n = 10$, 12). (M–P) In cKO^{Pvalb} mice, a lower dose of PTZ (50 mg/kg) induced more EEG seizure activity as measured by reduced onset ($t_{13.17} = 5.29$, $P = 1.4 \times 10^{-4}$, $n = 7$, 9) and increased percentage duration of electrographic seizures ($t_{9.27} = 2.61$, $P = 0.0277$, $n = 7$, 9). Representative EEG traces of seizure in cKO^{Pvalb} and control mice. (Scale bar, 20 μ m). The stratum oriens layer (A and E) and the pyramidal cell layer (I) of the hippocampal CA1 region were used for the immunofluorescence imaging and quantification. A two-tailed unpaired *t* test with Welch's correction was used to compare two groups. Data are mean \pm SEM.

mice remained unchanged (Fig. 4G). The intensity of WFA staining was higher in 4E-BP2 cKO^{Pvalb} mice than in controls (an increase of $42.31 \pm 13.43\%$ in WFA intensity in 4E-BP2 cKO^{Pvalb}; Fig. 4H). These results indicate that 4E-BP2 ablation reduces the number of parvalbumin neurons in the hippocampus and changes the PNNs organization.

Human *Pik3ca*^{H1047R} Mutation in PVALB⁺ Neurons Increases Seizure Susceptibility. Since mTORC1 signaling in PVALB⁺ neurons modulates the threshold for PTZ-induced epileptiform seizures, we examined the effect of enhanced PI3K activity in PVALB⁺ neurons by generating a heterozygous conditional mutant mouse harboring a germline *Pik3ca* allele with an *H1047R* mutation in PVALB⁺ neurons (*Pik3ca*^{H1047R-Pvalb}; Fig. 5A). The *H1047R* mutation hyperactivates the catalytic p110 α subunit of PI3K in PVALB⁺ neurons. We assessed AKT kinase activity, which is downstream of PI3K, in PVALB⁺ neurons in *Pik3ca*^{H1047R-Pvalb} mice by measuring the phosphorylation of AKT at threonine 308 (Thr308) in the activation loop motif. AKT phosphorylation on Thr308 was significantly increased in PVALB⁺ neurons in the *Pik3ca*^{H1047R-Pvalb} mice as compared with control animals ($49.83 \pm 12.65\%$ increase in AKT phosphorylation; Fig. 5B and C). Also, the phosphorylation of S6 protein kinase (S6K) at Thr389 was significantly increased in the PVALB⁺ neurons of *Pik3ca*^{H1047R-Pvalb} mice ($68.12 \pm 24.27\%$ increase in S6K phosphorylation; Fig. 5D and E). The phosphorylation of 4E-BP2

was not assessed due to the lack of immunohistochemistry-compatible antibodies. The *Pik3ca*^{H1047R-Pvalb} conditional knockin mice exhibited an increase in mortality and duration of PTZ-evoked seizures and a shortened seizure onset as compared with control groups ($28.21 \pm 7.99\%$ decrease in latency to the first seizure and $78.25 \pm 24.02\%$ increase in total seizure duration; Fig. 5F–H). In conclusion, the PVALB⁺ neuron-specific activating mutation (H1047R) of PI3K increased mTORC1 activity and promoted susceptibility to PTZ-induced seizures.

Discussion

Aberrant activation of the mTORC1 pathway is implicated in numerous brain disorders, including ASD and epilepsy (23, 52). Studies in animal models have established a causal link between mTORC1 hyperactivation and epileptogenesis (53). The mTORC1 signaling also modulates the eEF2K/eEF2 pathway, known to be involved in seizure susceptibility (54). We show that the up-regulation of mTORC1/eIF4E-dependent protein synthesis lowers the threshold for the induction of epileptic seizures. Mice lacking mTORC1-downstream translational repressors 4E-BP1 and 4E-BP2 showed no spontaneous visible seizures, but exhibit shortened latency to the first PTZ-induced seizure, increased duration of epileptic events, and elevated mortality, demonstrating that stimulation of eIF4E-dependent mRNA translation promotes epileptogenesis. This conclusion is consistent with a recent study showing that knockdown of eIF4E rescues the epileptic

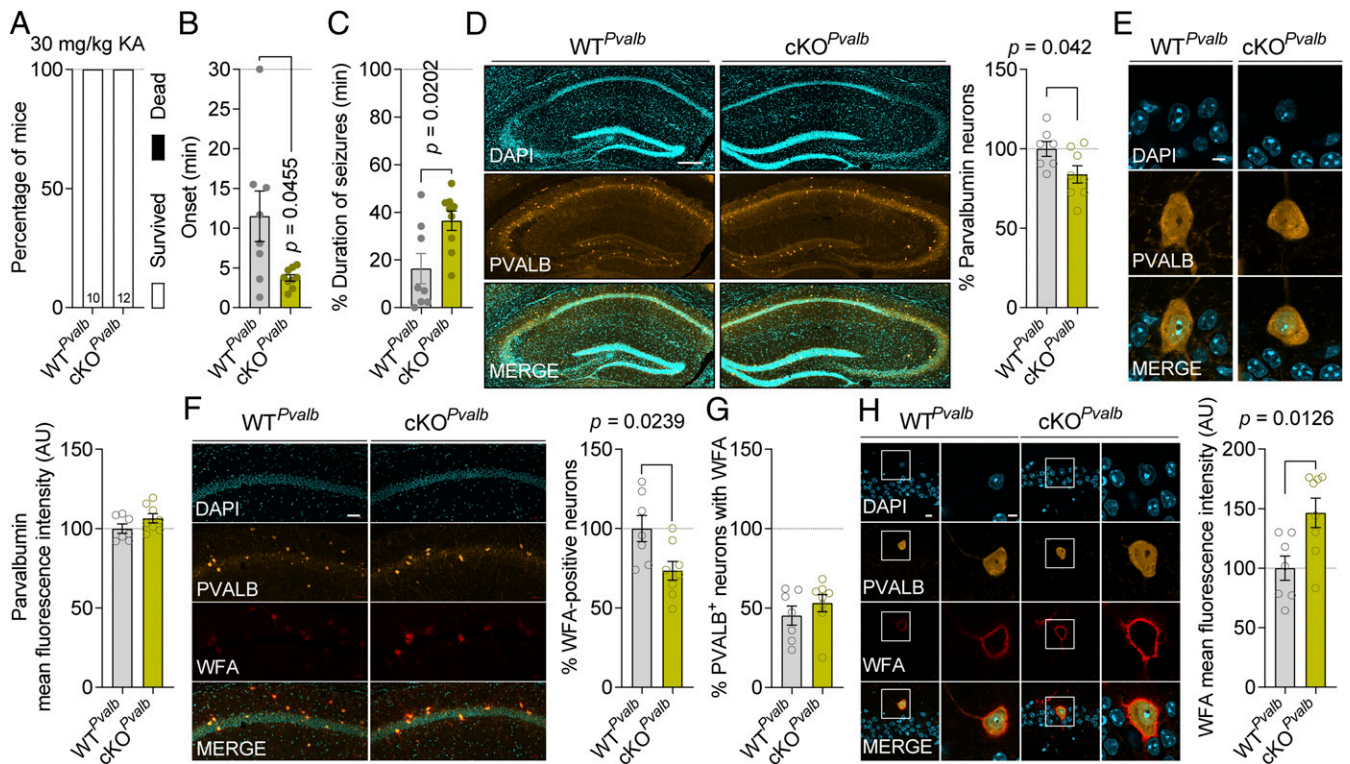


Fig. 4. *Eif4ebp2^{Pvalb}* mice exhibit increased sensitivity to kainic acid and reduced number of parvalbumin-positive neurons and WFA/PNNs ratio in the hippocampus. (A–C) Administration of 30 mg/kg KA significantly reduces the behavioral seizure latency ($t_{7,224} = 2.413$, $P = 0.0455$, $n = 8, 9$) and increases seizure events in cKO^{Pvalb} mice ($t_{12,14} = 2.67$, $P = 0.02$, $n = 8, 9$). (D) Representative hippocampus sections of control and cKO^{Pvalb} mice. (Scale bar, 200 μ m.) The cKO^{Pvalb} mice have a significantly lower percentage of PVALB⁺ neurons in the hippocampus than the control mice ($t_{12,93} = 2.261$, $P = 0.042$, $n = 7, 8$). (E) The parvalbumin expression levels are identical in the control and cKO^{Pvalb} mice hippocampus ($t_{12,92} = 1.583$, $P = 0.138$, $n = 7, 8$). (F) A reduced percentage of PVALB⁺ neurons also decreased the density of the PNNs surrounding PVALB⁺ neurons in the hippocampus of cKO^{Pvalb} mice ($t_{11,23} = 2.611$, $P = 0.0239$, $n = 7, 8$). (Scale bar, 50 μ m.) (G) However, the PNNs/PVALB⁺ ratio remains unchanged between the hippocampus of control and cKO^{Pvalb} mice ($t_{12,58} = 0.967$, $P = 0.352$, $n = 7, 8$). (H) In cKO^{Pvalb} mice, PNNs show stronger WFA⁺ signal as compared with control mice ($t_{12,84} = 2.9$, $P = 0.0126$, $n = 7, 8$). (Scale bar, 20 μ m.) The pyramidal layer of the hippocampal CA1 region was used for the immunofluorescence imaging and quantification of E and H. A two-tailed unpaired t test with Welch's correction was used to compare two groups. Data are mean \pm SEM.

phenotype in a mouse model of FMCD caused by mTORC1 hyperactivation (5).

4E-BP1, 4E-BP2, and 4E-BP3 act similarly, but differ in tissue distribution; 4E-BP2 is the predominant paralog expressed in the mammalian brain (39) (Fig. 1A). Loss of 4E-BP2 engenders ASD-like phenotypes such as impairment in social interaction, altered communication, and repetitive/stereotyped behavior (12). It also causes an increase in the ratio of excitatory to inhibitory synaptic inputs, a common pathogenic mechanism in both ASD and epilepsy. Our data show that the ablation of 4E-BP2, but not 4E-BP1, promotes epileptogenesis. This finding supports the notion that both ASD and epileptic disorders, which often share underlying pathophysiological mechanisms, can be caused by 4E-BP2-dependent mechanisms.

Revealing distinct cell types in the brain via which hyperactivated mTORC1 signaling promotes epileptogenesis is critical for understanding epilepsy pathophysiology and identifying specific therapeutic targets. Our results show that loss of 4E-BP2 in inhibitory, but not excitatory, neurons lowers the threshold and increases the seizure severity in cKO^{Nkx2.1} and cKO^{Gad2} mice. Despite being a small fraction of all cortical neurons (~10 to 20%), inhibitory interneurons are central for the regulation of neuronal circuit excitability as each inhibitory interneuron controls the activity of numerous excitatory pyramidal neurons (55–57). The deficit in the development or function of GABAergic interneurons engender excitation (E) to inhibition (I) imbalance and brain circuit hyperexcitability and is one of the prevalent causes of

epileptiform activities and seizures (12, 58, 59). Notably, deletion of 4E-BP2 in inhibitory, but not excitatory neurons causes ASD-like behaviors (60), further underscoring the similarities in mechanisms by which mTORC1/4E-BP2-dependent translation engenders ASD and epileptic phenotypes.

GABAergic interneurons exhibit a remarkable diversity in morphology, electrical discharge properties, and molecular marker expression patterns (61, 62). We identified PVALB⁺ interneurons as a key player in epileptogenesis, as the deletion of 4E-BP2 in PVALB⁺ interneurons but not in other subtypes, is sufficient to promote epileptogenesis. Parvalbumin-positive inhibitory interneurons (composing ~40% of all inhibitory neurons) are fast-spiking neurons that show little spike frequency adaptation and powerfully suppress the activity of the excitatory neurons via somatic inhibition (63). Dysfunction of parvalbumin interneurons resulting from developmental abnormalities, genetic disorders, or insult (e.g., trauma, anoxia, tumor) is often associated with cognitive deficits and epilepsy (64–66). Optogenetic activation of parvalbumin interneurons inhibits spontaneous seizures in a mouse model of temporal lobe epilepsy (67, 68), further supporting the central role of this cell population in the pathophysiology of epilepsy.

In 4E-BP2 cKO^{Pvalb} mice, the number of PVALB⁺ neurons was reduced in the adult hippocampus. The decreased number of inhibitory parvalbumin neurons in 4E-BP2 cKO^{Pvalb} mice can lead to neuronal network hyperexcitability and contribute to the increased susceptibility to epileptic seizures. Loss of inhibitory Purkinje neurons in mice with the hyperactivation of mTORC1

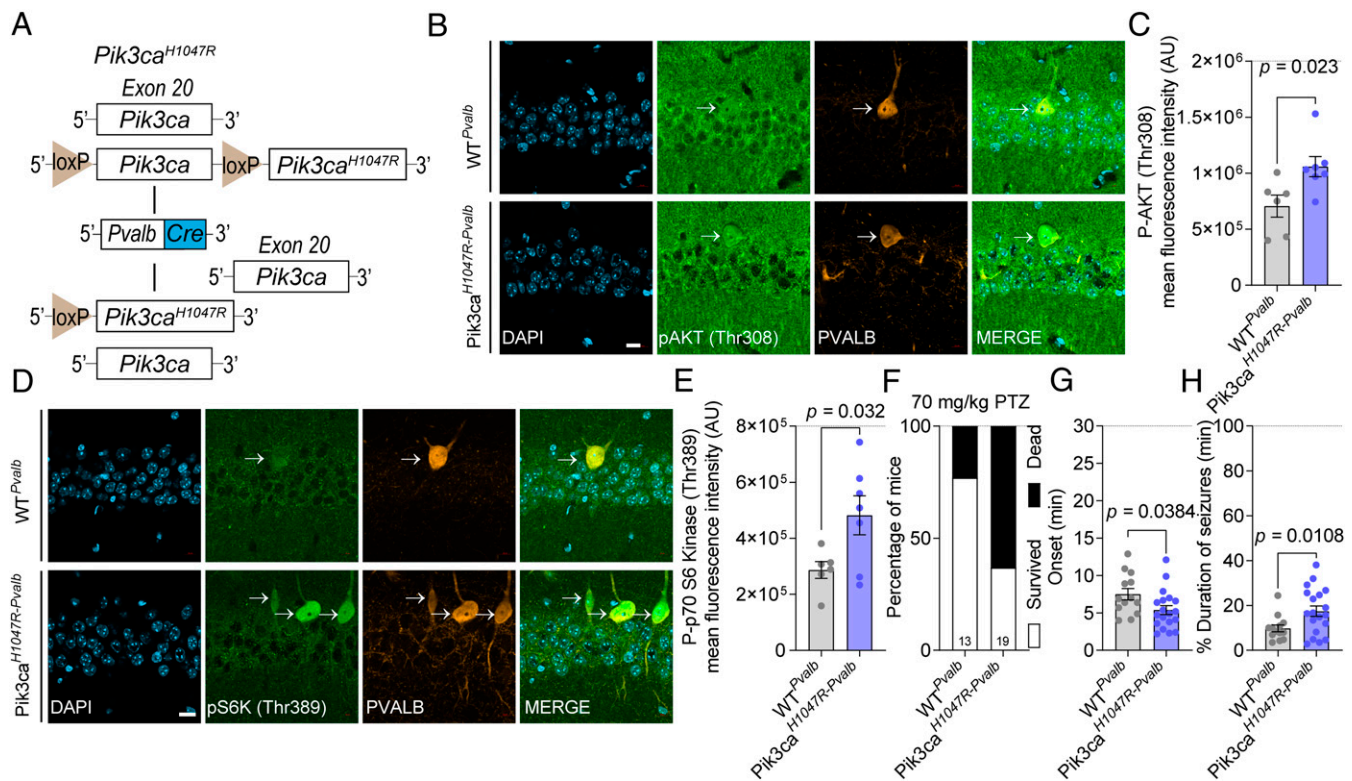


Fig. 5. An activating mutation of human *Pik3ca* in PVALB⁺ neurons is sufficient to lower the PTZ-induced seizure threshold in mice. (A) The genetic schematic of the conditional *Pik3ca*^{H1047R} mutation in PVALB⁺ neurons. (B–E) Immunofluorescent staining shows increased p-AKT Thr308 ($t_{10.64} = 2.653$, $P = 0.023$, $n = 6$, 7) and p-S6K Thr389 ($t_{8.081} = 2.58$, $P = 0.032$, $n = 6$, 7) as a result of a conditional *Pik3ca*^{H1047R} mutation in PVALB⁺ neurons. (F–H) The increased PI3K activity in *Pik3ca*^{H1047R-Pvalb} is sufficient to increase PTZ-induced seizures. The mortality was increased, the onset of seizures was significantly reduced ($t_{25.07} = 2.185$, $P = 0.0384$, $n = 13$, 19), and percentage duration of seizure was significantly increased ($t_{28.80} = 2.726$, $P = 0.0108$, $n = 13$, 19) in *Pik3ca*^{H1047R-Pvalb} as compared with WT^{Pvalb} control mice following the 70 mg/kg PTZ injection. (Scale bar, 20 μ m.) The pyramidal layer of the hippocampal CA1 region was used for the immunofluorescence imaging and quantification of B and D. A two-tailed unpaired *t* test with Welch's correction was used to compare two groups. Data are mean \pm SEM.

has been previously reported in the cerebellum of Purkinje cell TSC1 mutants (69). Our study raises the possibility that the loss is mediated by mTORC1/4E-BP2-dependent mechanisms.

PNNs, which develop postnatally, restrict neuronal plasticity in adulthood and stabilize neuronal circuits by maintaining the activity of parvalbumin interneurons (49). Removal of PNNs using genetic (e.g., deletion of aggrecan) (70) or enzymatic approaches (chondroitinase ABC [chABC]) (71) results in enhanced neuronal activity and elevated neuroplasticity (50, 51). Degradation of PNNs by chABC increases the susceptibility to PTZ-induced seizures (72), and change in the composition of PNNs (decrease in the 4-sulfation/6-sulfation ratio) is associated with increased susceptibility to KA-induced seizures (73). Thus, the observed changes in PNNs in 4E-BP2 cKO^{Pvalb} mice, as evidenced by increased WFA staining, might be one of the mechanisms by which the activation of 4E-BP2-dependent translation lowers the threshold for the induction of epileptic seizures. Whether protein components of PNNs (e.g., aggrecan, brevican, versican, neurocan) are under the direct 4E-BP2-dependent translation control or other mechanisms are involved remains unknown and should be investigated.

Since 4E-BP2 deletion engenders the formation of eIF4F complex and translation initiation, targeting eIF4F complex is an attractive strategy to normalize 4E-BP2-dependent translation and reverse seizure phenotype in both 4E-BP2 cKO^{Pvalb} and *Pik3ca*^{H1047R-Pvalb} mouse models and humans with eIF4E-dependent epilepsy. This can be achieved using a small molecule like 4EGI-1, which disrupts the eIF4E/eIF4G interaction and has been shown to rescue ASD-like phenotypes in mice with enhanced

eIF4F activity (12, 74). All the experiments in this study were performed in male mice; therefore, it remains to be determined whether enhancing 4E-BP2-dependent translation in parvalbumin neurons in female animals also lowers seizure thresholds.

In summary, we show that the translational repressor 4E-BP2 in PVALB⁺ fast-spiking interneurons plays a key role in regulating susceptibility to epileptic seizures. These results are consistent with the notion that activating mutations of PI3K/AKT/mTORC1/eIF4E-dependent translation acts in a cell type-specific manner to promote epileptogenesis. Our results foster the idea of therapeutically targeting eIF4E in epileptic disorders associated with dysregulated translation in the brain.

Materials and Methods

Animals and Environment. In this study, we used general *Eif4ebp1/2/3* triple knockout (*Eif4ebp1/2/3*^{-/-}) (43), *Eif4ebp1* knockout (*Eif4ebp1*^{-/-}), *Eif4ebp2* knockout (*Eif4ebp2*^{-/-}) (45), and wild-type mice (all on pure C57BL/6 genetic background). Neuronal subtype-specific *Eif4ebp2* conditional knockout (cKO) mice were generated by breeding *Eif4ebp2*^{flx/flx} floxed mice (60) with Cre⁺ transgenic lines driven by either the *Emx1*, *Camk2a*, *Nx2.1*, *Gad2*, *Pvalb*, *VIP*, or *Sst* promoters (all on C57BL/6 genetic background). We first bred *Eif4ebp2*^{flx/flx} with neuronal subtype-specific Cre mice to generate Cre-positive, *Eif4ebp2*^{flx/+} heterozygous mice. *Eif4ebp2*^{flx/+}; Cre positive mice were then bred with *Eif4ebp2*^{flx/flx} mice to generate homozygous *Eif4ebp2* cKO mice and neuronal subtype-specific X-Cre-positive control mice. *Pik3ca*^{H1047R} mice (75) were mated with *Pvalb*-Cre⁺ transgenic mice, which selectively express Cre recombinase (Cre) in parvalbumin neurons. Heterozygous *Pvalb*-Cre⁺; *Pik3ca*^{H1047R/WT} were used as mutants. We used adult (2- to 3-mo-old, weight range 26 to 30 g) male mice for all experiments. Mice

were housed in standard laboratory cages (four to five mice per cage) under conditions of controlled temperature and illumination (12-h light-dark cycle, with lights on at 07:00 AM and off at 07:00 PM). The ad libitum amount of food and water was provided to the mice and monitored regularly. Cages were maintained in ventilated racks in temperature (20 to 21 °C)- and humidity (~55%)-controlled rooms. Mice were housed under standard conditions at the Goodman Cancer Research Centre (GCRC), the Montreal Neurological Institute, and the University of Montréal animal facility. All experiments were carried out under the Canadian Council on Animal Care (CCAC) guidelines and were approved by both McGill University and the University of Montréal. The experiments were conducted during the light phase of the cycle, and the experimenter was blind to the genotype for all behavioral tests. Anesthetized mice were killed by exposing them to carbon dioxide as per CCAC guideline recommendations, followed by cervical dislocation.

Induction and Analysis of Seizures. Adult mice were injected with different doses of PTZ: 50, 60, and 70 mg/kg s.c. (Sigma CAS- 54-95-5) and KA: 10, 20, and 30 mg/kg s.c. (Tocris Biosciences UK-0222) to determine the optimal dosage for the inducing generalized clonic or tonic seizures. Seizures were videorecorded for 30 min, and behaviors were scored by an observer blinded to genotype. The times of seizure onset and seizure duration, and the percentage of mice survival and death, were determined for an individual group, compared with the observations from the control group. At the end of the experiments, all mice were killed as per CCAC guidelines. None of the tested mouse lines exhibited spontaneous visible seizures.

Electrode Implantation, EEG Recordings, and Analysis. Anesthetized mice (isoflurane) were unilaterally implanted with a bipolar electrode (20 to 35 k Ω) into the CA3 region (anteroposterior, -2.85 mm relative to bregma; lateral, -3.0 mm; ventral, -4.0 mm), and an angled reference electrode (5 to 10 k Ω) was inserted above the contralateral hemisphere cortex, both electrodes secured in place by dental acrylic cement. Following the surgery, the incision site was treated with chloramphenicol and lidocaine (5%; Odan). Buprenorphine (0.1 mg/kg), carprofen (20 mg/kg), enrofloxacin (5 mg/kg), and saline were administered subcutaneously for perioperative pain relief. One week after the surgery, electrodes were connected to a multichannel cable and electrical swivel (Commutator SL 18C, HRS Scientific). Continuous EEG activity was recorded from 24 h before to 3 h following intraperitoneal (i.p.) injection of 50 mg/kg PTZ. EEGs were recorded and amplified by an interface kit (Mobile 36ch LTM ProAmp, Stellate) and low-pass filtered at 500 Hz with a 2,000-Hz sampling rate per channel. The data were collected using monitoring software (Harmonie, Stellate). Mice showing a decrease in body weight 1 wk postimplantation were not used for EEG recordings.

Stereotaxic Surgery: Infusion of AAV into Adult Mouse Brain. Mice were anesthetized under isoflurane (1 to 3% in oxygen) and placed in a stereotaxic head frame on a temperature-controlled heating pad. Anesthetized mice were mounted on a Kopf stereotaxic frame and maintained with 1.5% isoflurane, a small incision was made, and the skull was exposed to drill a small hole above the hippocampus of each hemisphere. A total of 0.5 μ L of AAV expressing AAV9-EF1 α -DIO-EYFP-WPRE-hGH (3.3e13 GC/mL; Addgene 27056-AAV9) was injected over 10 min per CA1, using a 5- μ L Hamilton syringe with a 23-G needle attached to a stereotaxic infusion pump. The CA1 coordinates (anteroposterior, -1.90 mm relative to bregma; lateral, ± 1.0 mm; ventral, -1.50 mm) were used according to the Franklin and Paxinos Atlas (76). The needle was kept in place for 5 min before and after infusion to minimize fluid retraction. After the surgery, virus-injected mice were allowed to recover in their home cages for 2 to 3 wk before any experiments were conducted.

Western Blotting. Hippocampus was lysed in RIPA buffer (50 mM Tris-HCl pH 7.4, 150 mM NaCl, 1% Nonidet P-40, 0.1% sodium dodecyl sulfate (SDS), 0.5% sodium deoxycholate, 5 mM ethylenediaminetetraacetic acid (EDTA) pH

8.0, 1 mM ethylene glycol tetraacetic acid (EGTA) pH 8.0, 10 mM NaF, 1 mM β -glycerophosphate, and 1 mM sodium orthovanadate) with Halt protease and phosphatase inhibitor mixture (Thermo Fisher Scientific, 78440). Proteins were resolved by precast gradient gels (Thermo Fisher Scientific) and transferred to nitrocellulose membranes. The membranes were blocked with 3% bovine serum albumin (BSA) in tris buffer saline (TBS) containing 0.1% Tween-20 (TBST) for 1 h at room temperature and washed four times in TBST before immunoblotting was performed. The membranes were incubated with primary antibodies against 4E-BP1 (53H11; Cell Signaling, mAb 96445), 4E-BP2 (Cell Signaling Technology, CST-28455), and anti- β -actin antibody (clone AC-15; Sigma-Aldrich, A5441) in TBST overnight at 4 °C. Immunoreactivity was detected by enhanced chemiluminescence (plus-ECL, PerkinElmer, Inc.). Quantification of immunoblots was performed using a charge-coupled device (CCD) camera and Quantity One software (Bio-Rad). Membranes were stripped in 25 mM glycine-HCl pH 2.0 and 1% SDS for 30 min at room temperature and then washed four times with TBST before reprobing. Each sample was measured relative to the background, and values were normalized against β -actin.

Immunohistochemistry and Image Analysis. Mice were anesthetized with isoflurane (1 to 3% in oxygen) and then perfused with ice-cold phosphate buffer 0.1 M (PB) followed by cold 4% paraformaldehyde (PFA). Brains were fixed overnight in 4% PFA and cryoprotected sequentially in 20 mL of 10%, 20%, and 30% sucrose in phosphate buffered saline (PBS) at 4 °C. The 40- μ m-thick sections were cut on a cryostat and blocked in 20% normal goat serum (NGS) containing 0.1% Triton X-100 and incubated overnight with primary antibodies against 4E-BP2 (1:400, Cell Signaling Technology, CST 28455), Camk2 α (Cba-2; 1:1,000, Invitrogen 13-730), GAD67 (1:1,000, Millipore MAB5406), parvalbumin (1:1,000, Sigma P3088 and 1:1,000, Synaptic Systems 195004), somatostatin (1:100, Millipore MAB354), p-AKT (Thr308; 1:500, Cell Signaling Technology, CST 2965), p-p70 S6K (Thr389; 1:500, Cell Signaling Technology, CST 9205), and WFA (20 μ g/mL, Vector Labs B 1355) diluted in 2% NGS in PBS at 4 °C. The sections were rinsed three times for 10 min in PBS and incubated with secondary antibodies (Alexa-488, 1:400, Invitrogen, mouse-A11001 and rabbit-A11034; Alexa-546, 1:400, Invitrogen, mouse-A11030 and rabbit-A11035; Alexa-647, 1:400, Invitrogen A21247) in blocking buffer for 1 h at room temperature. Sections were rinsed three times for 10 min in PBS before being mounted on slides using SlowFade Gold antifade mountant (Thermo Fisher Scientific). The slices were imaged using a confocal microscope (Zeiss LSM 880 with Airyscan). All images were acquired under identical conditions. Image processing was performed with ImageJ (NIH).

Statistical Analysis. The statistical comparisons in this study were performed using GraphPad Prism 8.00 (GraphPad Prism Software Inc.). The two-tailed unpaired Student's *t* test with Welch's correction was used to determine statistically significant differences between the two groups. The statistical significance differences at different time points were determined using a two-way repeated measure ANOVA or mixed-effects model (restricted maximum likelihood [REML]). The post hoc test (Tukey's or Sidak's, α -level of 0.05 and $P < 0.05$) was used to compare individual groups. Data are presented as mean \pm SEM.

Data Availability. All study data are included in the article and/or supporting information.

ACKNOWLEDGMENTS. Funding was provided by Canadian Institutes of Health Research (CIHR) Grants FDN-148423 (to N. Sonenberg), PJT-162412 (to A.K.), and MOP130328 (to M.A.). Support to R.S. was provided by Richard and Edith Strauss Postdoctoral Fellowships in Medicine. We thank the N. Sonenberg laboratory members, specifically I. Harvey, A. Lafrance, A. Sylvestre, and E. Migon, for support with animals and resources. J.-C.L. is supported by CIHR Project Grant PJT-153311 and by the Canada Research Chair in Cellular and Molecular Neurophysiology (CRC-950-231066).

1. W. H. Theodore *et al.*, Epilepsy in North America: A report prepared under the auspices of the global campaign against epilepsy, the International Bureau for epilepsy, the international league against epilepsy, and the World Health organization. *Epilepsia* **47**, 1700–1722 (2006).
2. O. Devinsky *et al.*, Epilepsy. *Nat. Rev. Dis. Primers* **4**, 18024 (2018).
3. M. Mula, J. W. Sander, Psychosocial aspects of epilepsy: A wider approach. *BJPsych Open* **2**, 270–274 (2016).
4. E. Beghi, Social functions and socioeconomic vulnerability in epilepsy. *Epilepsy Behav.* **100**, 106363 (2019).

5. J. K. Kim *et al.*, Brain somatic mutations in MTOR reveal translational dysregulations underlying intractable focal epilepsy. *J. Clin. Invest.* **129**, 4207–4223 (2019).
6. J. K. Kim, J. H. Lee, Mechanistic target of rapamycin pathway in epileptic disorders. *J. Korean Neurosurg. Soc.* **62**, 272–287 (2019).
7. S. Tahmasebi, A. Khoutorsky, M. B. Mathews, N. Sonenberg, Translation deregulation in human disease. *Nat. Rev. Mol. Cell Biol.* **19**, 791–807 (2018).
8. I. Gantois *et al.*, Metformin ameliorates core deficits in a mouse model of fragile X syndrome. *Nat. Med.* **23**, 674–677 (2017).

9. M. Neves-Pereira *et al.*, Deregulation of EIF4E: A novel mechanism for autism. *J. Med. Genet.* **46**, 759–765 (2009).
10. P. H. Iffland II, P. B. Crino, Focal cortical dysplasia: Gene mutations, cell signaling, and therapeutic implications. *Annu. Rev. Pathol.* **12**, 547–571 (2017).
11. W. S. Sossin, M. Costa-Mattioli, Translational control in the brain in health and disease. *Cold Spring Harb. Perspect. Biol.* **11**, a032912 (2019).
12. C. G. Gkogkas *et al.*, Autism-related deficits via dysregulated eIF4E-dependent translational control. *Nature* **493**, 371–377 (2013).
13. L. de la Torre-Ubieta, H. Won, J. L. Stein, D. H. Geschwind, Advancing the understanding of autism disease mechanisms through genetics. *Nat. Med.* **22**, 345–361 (2016).
14. M. Morita *et al.*, mTOR coordinates protein synthesis, mitochondrial activity and proliferation. *Cell Cycle* **14**, 473–480 (2015).
15. M. Morita *et al.*, mTORC1 controls mitochondrial activity and biogenesis through 4E-BP-dependent translational regulation. *Cell Metab.* **18**, 698–711 (2013).
16. R. Citraro, A. Leo, A. Constanti, E. Russo, G. De Sarro, mTOR pathway inhibition as a new therapeutic strategy in epilepsy and epileptogenesis. *Pharmacol. Res.* **107**, 333–343 (2016).
17. A. G. Mazumder, V. Patial, D. Singh, Mycophenolate mofetil contributes to down-regulation of the hippocampal interleukin type 2 and 1β mediated PI3K/AKT/mTOR pathway hyperactivation and attenuates neurobehavioral comorbidities in a rat model of temporal lobe epilepsy. *Brain Behav. Immun.* **75**, 84–93 (2019).
18. A. Roy *et al.*, Mouse models of human PIK3CA-related brain overgrowth have acutely treatable epilepsy. *eLife* **4**, e12703 (2015).
19. E. Russo, R. Citraro, A. Constanti, G. De Sarro, The mTOR signaling pathway in the brain: Focus on epilepsy and epileptogenesis. *Mol. Neurobiol.* **46**, 662–681 (2012).
20. L. H. Zeng, L. Xu, D. H. Gutmann, M. Wong, Rapamycin prevents epilepsy in a mouse model of tuberous sclerosis complex. *Ann. Neurol.* **63**, 444–453 (2008).
21. C. H. Kwon, X. Zhu, J. Zhang, S. J. Baker, mTOR is required for hypertrophy of Pten-deficient neuronal soma in vivo. *Proc. Natl. Acad. Sci. U.S.A.* **100**, 12923–12928 (2003).
22. L. H. Zeng *et al.*, Tsc2 gene inactivation causes a more severe epilepsy phenotype than Tsc1 inactivation in a mouse model of tuberous sclerosis complex. *Hum. Mol. Genet.* **20**, 445–454 (2011).
23. L. H. Nguyen, T. Mahadeo, A. Bordey, mTOR hyperactivity levels influence the severity of epilepsy and associated neuropathology in an experimental model of tuberous sclerosis complex and focal cortical dysplasia. *J. Neurosci.* **39**, 2762–2773 (2019).
24. P. H. Iffland II, V. Carson, A. Bordey, P. B. Crino, GATORopathies: The role of amino acid regulatory gene mutations in epilepsy and cortical malformations. *Epilepsia* **60**, 2163–2173 (2019).
25. F. Qaiser, R. K. C. Yuen, D. M. Andrade, Genetics of epileptic networks: From focal to generalized genetic epilepsies. *Curr. Neurol. Neurosci. Rep.* **20**, 46 (2020).
26. C. J. Yuskaitis *et al.*, Chronic mTORC1 inhibition rescues behavioral and biochemical deficits resulting from neuronal Depdc5 loss in mice. *Hum. Mol. Genet.* **28**, 2952–2964 (2019).
27. M. Trivisano *et al.*, Developmental and epileptic encephalopathy due to SZT2 genomic variants: Emerging features of a syndromic condition. *Epilepsy Behav.* **108**, 107097 (2020).
28. L. H. Nguyen *et al.*, mTOR inhibition suppresses established epilepsy in a mouse model of cortical dysplasia. *Epilepsia* **56**, 636–646 (2015).
29. V. Grande, G. Manassero, A. Vercelli, Neuroprotective and anti-inflammatory roles of the phosphatase and tensin homolog deleted on chromosome ten (PTEN) inhibition in a mouse model of temporal lobe epilepsy. *PLoS One* **9**, e114554 (2014).
30. S. Tokuda *et al.*, A novel Akt3 mutation associated with enhanced kinase activity and seizure susceptibility in mice. *Hum. Mol. Genet.* **20**, 988–999 (2011).
31. J. Zhou *et al.*, Pharmacological inhibition of mTORC1 suppresses anatomical, cellular, and behavioral abnormalities in neural-specific Pten knock-out mice. *J. Neurosci.* **29**, 1773–1783 (2009).
32. E. M. M. Svarrer, C. M. Fischer, M. G. Frederiksen, A. P. Born, C. E. Hoei-Hansen, Everolimus as adjunctive treatment in tuberous sclerosis complex-associated epilepsy in children. *Dan. Med. J.* **66**, A5582 (2019).
33. I. E. Overwater, A. B. Rietman, A. M. van Eeghen, M. C. Y. de Wit, Everolimus for the treatment of refractory seizures associated with tuberous sclerosis complex (TSC): Current perspectives. *Ther. Clin. Risk Manag.* **15**, 951–955 (2019).
34. S. S. Schalm, J. Blenis, Identification of a conserved motif required for mTOR signaling. *Curr. Biol.* **12**, 632–639 (2002).
35. H. Nojima *et al.*, The mammalian target of rapamycin (mTOR) partner, raptor, binds the mTOR substrates p70 S6 kinase and 4E-BP1 through their TOR signaling (TOS) motif. *J. Biol. Chem.* **278**, 15461–15464 (2003).
36. N. Sonenberg, A. G. Hinnebusch, New modes of translational control in development, behavior, and disease. *Mol. Cell* **28**, 721–729 (2007).
37. X. M. Ma, J. Blenis, Molecular mechanisms of mTOR-mediated translational control. *Nat. Rev. Mol. Cell Biol.* **10**, 307–318 (2009).
38. M. Bidinosti *et al.*, Postnatal deamidation of 4E-BP2 in brain enhances its association with raptor and alters kinetics of excitatory synaptic transmission. *Mol. Cell* **37**, 797–808 (2010).
39. K. Tsukiyama-Kohara *et al.*, Adipose tissue reduction in mice lacking the translational inhibitor 4E-BP1. *Nat. Med.* **7**, 1128–1132 (2001).
40. J. H. Lee *et al.*, De novo somatic mutations in components of the PI3K-AKT3-mTOR pathway cause hemimegalencephaly. *Nat. Genet.* **44**, 941–945 (2012).
41. J. S. Lim *et al.*, Brain somatic mutations in MTOR cause focal cortical dysplasia type II leading to intractable epilepsy. *Nat. Med.* **21**, 395–400 (2015).
42. M. Nakashima *et al.*, Somatic Mutations in the MTOR gene cause focal cortical dysplasia type IIb. *Ann. Neurol.* **78**, 375–386 (2015).
43. D. Pearl *et al.*, 4E-BP-dependent translational control of *Irf8* mediates adipose tissue macrophage inflammatory response. *J. Immunol.* **204**, 2392–2400 (2020).
44. S. L. Hansen, B. B. Sperling, C. Sánchez, Anticonvulsant and antiepileptogenic effects of GABAA receptor ligands in pentylenetetrazole-kindled mice. *Prog. Neuro-psychopharmacol. Biol. Psychiatry* **28**, 105–113 (2004).
45. J. L. Banko *et al.*, The translation repressor 4E-BP2 is critical for eIF4F complex formation, synaptic plasticity, and memory in the hippocampus. *J. Neurosci.* **25**, 9581–9590 (2005).
46. M. Lévesque, M. Avoli, The kainic acid model of temporal lobe epilepsy. *Neurosci. Biobehav. Rev.* **37**, 2887–2899 (2013).
47. Q. Xu, M. Tam, S. A. Anderson, Fate mapping Nkx2.1-lineage cells in the mouse telencephalon. *J. Comp. Neurol.* **506**, 16–29 (2008).
48. P. J. Kiser, N. G. Cooper, G. D. Mower, Expression of two forms of glutamic acid decarboxylase (GAD67 and GAD65) during postnatal development of rat somatosensory barrel cortex. *J. Comp. Neurol.* **402**, 62–74 (1998).
49. J. W. Fawcett, T. Ohashi, T. Pizzorusso, The roles of perineuronal nets and the perinodal extracellular matrix in neuronal function. *Nat. Rev. Neurosci.* **20**, 451–465 (2019).
50. Q. Ye, Q. L. Miao, Experience-dependent development of perineuronal nets and chondroitin sulfate proteoglycan receptors in mouse visual cortex. *Matrix Biol.* **32**, 352–363 (2013).
51. H. Ueno, S. Suemitsu, M. Okamoto, Y. Matsumoto, T. Ishihara, Sensory experience-dependent formation of perineuronal nets and expression of Cat-315 immunoreactive components in the mouse somatosensory cortex. *Neuroscience* **355**, 161–174 (2017).
52. R. E. Dawson *et al.*, Functional screening of GATOR1 complex variants reveals a role for mTORC1 deregulation in FCD and focal epilepsy. *Neurobiol. Dis.* **134**, 104640 (2020).
53. A. P. Ostendorf, M. Wong, mTOR inhibition in epilepsy: Rationale and clinical perspectives. *CNS Drugs* **29**, 91–99 (2015).
54. C. Heise *et al.*, eEF2K/eEF2 pathway controls the excitation/inhibition balance and susceptibility to epileptic seizures. *Cereb. Cortex* **27**, 2226–2248 (2017).
55. J. Chu, S. A. Anderson, Development of cortical interneurons. *Neuropsychopharmacology* **40**, 16–23 (2015).
56. K. A. Pelkey *et al.*, Hippocampal GABAergic inhibitory interneurons. *Physiol. Rev.* **97**, 1619–1747 (2017).
57. I. Soltesz, A. Losonczy, CA1 pyramidal cell diversity enabling parallel information processing in the hippocampus. *Nat. Neurosci.* **21**, 484–493 (2018).
58. G. Rippon, J. Brock, C. Brown, J. Boucher, Disordered connectivity in the autistic brain: Challenges for the “new psychophysiology”. *Int. J. Psychophysiol.* **63**, 164–172 (2007).
59. M. A. Dichter, G. F. Ayala, Cellular mechanisms of epilepsy: A status report. *Science* **237**, 157–164 (1987).
60. S. Wiebe *et al.*, Inhibitory interneurons mediate autism-associated behaviors via 4E-BP2. *Proc. Natl. Acad. Sci. U.S.A.* **116**, 18060–18067 (2019).
61. J. Righes Marafiga, M. Vendramin Pasquetti, M. E. Calcagnotto, GABAergic interneurons in epilepsy: More than a simple change in inhibition. *Epilepsy Behav.*, <https://doi.org/10.1016/j.yebep.2020.106935> (2020).
62. V. Sharma *et al.*, eIF2 α controls memory consolidation via excitatory and somatostatin neurons. *Nature* **586**, 412–416 (2020).
63. B. Rudy, G. Fishell, S. Lee, J. Hjerling-Leffler, Three groups of interneurons account for nearly 100% of neocortical GABAergic neurons. *Dev. Neurobiol.* **71**, 45–61 (2011).
64. E. Rössignol, Genetics and function of neocortical GABAergic interneurons in neurodevelopmental disorders. *Neural Plast.* **2011**, 649325 (2011).
65. X. Jiang, M. Lachance, E. Rössignol, Involvement of cortical fast-spiking parvalbumin-positive basket cells in epilepsy. *Prog. Brain Res.* **226**, 81–126 (2016).
66. X. Jiang *et al.*, Remodeled cortical inhibition prevents motor seizures in generalized epilepsy. *Ann. Neurol.* **84**, 436–451 (2018).
67. E. Krook-Magnuson, C. Armstrong, M. Oijala, I. Soltesz, On-demand optogenetic control of spontaneous seizures in temporal lobe epilepsy. *Nat. Commun.* **4**, 1376 (2013).
68. E. Krook-Magnuson, G. G. Szabo, C. Armstrong, M. Oijala, I. Soltesz, Cerebellar directed optogenetic intervention inhibits spontaneous hippocampal seizures in a mouse model of temporal lobe epilepsy. *eNeuro* **1**, ENEURO.0005-14.2014 (2014).
69. P. T. Tsai *et al.*, Autistic-like behaviour and cerebellar dysfunction in Purkinje cell Tsc1 mutant mice. *Nature* **488**, 647–651 (2012).
70. D. Rowlands *et al.*, Aggrecan directs extracellular matrix-mediated neuronal plasticity. *J. Neurosci.* **38**, 10102–10113 (2018).
71. T. Pizzorusso *et al.*, Reactivation of ocular dominance plasticity in the adult visual cortex. *Science* **298**, 1248–1251 (2002).
72. E. K. Rankin-Gee *et al.*, Perineuronal net degradation in epilepsy. *Epilepsia* **56**, 1124–1133 (2015).
73. N. Yutsudo, H. Kitagawa, Involvement of chondroitin 6-sulfation in temporal lobe epilepsy. *Exp. Neurol.* **274**, 126–133 (2015).
74. E. Santini *et al.*, Exaggerated translation causes synaptic and behavioural aberrations associated with autism. *Nature* **493**, 411–415 (2013).
75. K. M. Kinross *et al.*, An activating Pik3ca mutation coupled with Pten loss is sufficient to initiate ovarian tumorigenesis in mice. *J. Clin. Invest.* **122**, 553–557 (2012).
76. K. B. J. Franklin, G. Paxinos, *The Mouse Brain in Stereotaxic Coordinates* (Academic Press, USA, ed. 3, 2007).